Environmental Sciences Europe

RESEARCH

Open Access

Industrial oily wastewater treatment by microfiltration using silver nanoparticle-incorporated poly (acrylonitrile-styrene) membrane

Atef El Jery[1], Amimul Ahsan[2,3*], Saad Sh. Sammen[4], Abdallah Shanableh[5,6], Dinesh Sain[7], Andrés Alexis Ramírez-Coronel[8,9,10], Md. Alhaz Uddin[11], Mohammed Abdul Jaleel Maktoof[12], Md. Shafiquzzaman[13] and Nadhir Al-Ansari[14*]

Abstract

Membrane filtration exhibit operational limitations such as biofouling, which leads to concentration polarization and reduces permeability and selectivity, despite advantages such as low operating cost, high selectivity, and permeability. In recent years, the antibacterial properties of silver nanoparticles (AgNPs) have been investigated for improving membrane processes; however, the fouling phenomena in presence of AgNPs in the membrane matrix have not been fully discussed. Herein, the antifouling properties of a poly (acrylonitrile-styrene) copolymer incorporated with AgNPs were studied in a microfiltration membrane process. The Creighton method was used to synthesize AgNPs, and the effects of AgNPs on the porosity, morphology, pore size, mechanical strength, permeability, and selectivity of the membranes were investigated. Moreover, to investigate the biofouling of the obtained membranes, microfiltration of industrial oily wastewater was performed at constant pressure over three cycles. Using AgNPs in the membrane matrix resulted in enhanced antifouling properties of the copolymer membrane, which is related to the structure of the AgNPs in the casting solution, as proven by SAXS analysis. The results show that the CFU% for Staphylococcus aureus and E.coli reach 2% and 6%, respectively. Finally, the Derjaguin–Landau–Verwey–Overbeek (DLVO) thermodynamic model was applied to study the antifouling mechanism, correctly predict the separation behavior in the membrane, and design, simulate, and optimize the separation processes in the membrane separation plantsa. The DLVO model could predict the separation behavior in the synthesized membranes, and the poly(acrylonitrile-styrene) copolymer membranes containing AgNPs were proven have promising industrial wastewater treatment applications.

Keywords Copolymer membrane, Silver nanoparticles (AgNPs), Thermodynamic investigation, Oily wastewater, Membrane fouling, Microfiltration

*Correspondence:
Amimul Ahsan
ashikcivil@yahoo.com
Nadhir Al-Ansari
nadhir.alansari@ltu.se
Full list of author information is available at the end of the article

Introduction

Membrane technology is considered a promising for the treatment of wastewater, particularly the oily wastewater. The membranes are widely used to remove various pollutants; however, the key limitation of the current polymer membranes is biofouling [1, 2]. In the membrane fabrication procedure, polymer type and surface modification are among the most important factors determining the chemical and physical properties of the membrane. However, each membrane is suitable for specific application [3]. The basis for the selection of membranes is the mechanical, chemical, and thermal properties of the polymers [4].

The primary goal in the design of membrane processes is to produce a membrane that can create the maximum permeate flux with the maximum removal of substances from the feed and low fouling, which minimizes investment and operational costs. As a general rule, most polymers can be applied to produce membrane matrixes [5, 6]; however, according to process limitations, as well as the degree of membrane fouling, only a few polymers can be applied practically. Polymeric membranes have their own advantages and disadvantages according to their structural and material characteristics, thereby exhibiting different performances [7].

Membrane fouling, especially biofouling, is a bottleneck for the applications of membrane technology, and biofouling on the membrane surface can lead to a significant decrease in water permeability [8–10].

To modify the membrane surfaces, many attempts have been made via chemical modification, such as the grafting process; however, the reduction in membrane fouling has not been satisfactory [11–13]. Recently, nanotechnology has been used to improve water quality and treat wastewater [14], and the beneficial effects of nanoparticle-based membranes in reducing membrane fouling have recently been reported by many researchers [15]. Silver nanoparticles (AgNPs) have high antibacterial effects; they are highly toxic to microorganisms, including bacteria [16], fungi [17], and viruses [18]. In the last decade, AgNPs have attracted considerable attention owing to their disinfection and antibacterial properties [19], and they have been reported to damage the cell membrane [20]. Moreover, they can diffuse to the cell wall and subsequently change the cell membrane structure [21]. Furthermore, it is reported that the free radicals can be generated when AgNPs are in contact with bacteria [22]. However, the mechanism underlying the antimicrobial effects of AgNPs is not fully understood and remains debatable [23, 24]. In addition, the effect of AgNPs on the antifouling properties of fabricated membranes has not been fully investigated.

Many studies have investigated the addition of carbon nanotubes or metal oxide nanoparticles to polymer membranes, which led to improvement in permeability, fouling resistance, and permeation quality [25–27]. Therefore, the development of low-fouling antibacterial membrane processes has received considerable attention in the recent years. Despite the development of low-fouling and high-performance membranes using various nanoparticles [28–30], further research must be carried out to determine the performance of nanoparticle-based membranes.

A huge quantity of oily wastewater is produced by petroleum refining industry. The treatment methods of oily wastewater are summarized in 6 aspects, i.e. flotation, coagulation, biological treatment, membrane separation technology, combined technology and advanced oxidation process [31]. Furthermore, the application of combined technology is necessary for the removal of hazardous pollutants in high-strength oily wastewater [32].

In this study, along with the synthesis of AgNPs, the properties of polymer membranes, including poly (acrylonitrile-styrene) (SAN) composited with the synthesized AgNPs, were investigated. The performance of the fabricated membrane in industrial wastewater treatment using the microfiltration process was also studied via antibacterial activities and membrane biofouling experiments. Moreover, the antifouling mechanism was investigated using the Derjaguin–Landau–Verwey–Overbeek (DLVO) thermodynamic model, and a relationship was developed between the antifouling performance of the fabricated membranes and casting solution using the Small-angle X-ray scattering (SAXS) technique.

Material and methods

Membrane preparation

Copolymers consist of two or more types of monomer units with different properties. The properties of structural copolymers depend on the properties of their constituent units and their ratios. Therefore, by choosing different polymer units, different properties can be obtained in the membranes; in this regard, copolymers can be synthesized by combining hydrophobic and hydrophilic monomers [33, 34]. This provides a way to improve the properties and develop polymer applications. The poly (acrylonitrile-styrene) membrane was fabricated by dissolving the poly membrane (15 g) in 85 g of tetrahydrofuran (THF) and stirring for 24 h at 30 °C under atmospheric pressure. After obtaining a homogeneous and clear solution, it was stored at 30 °C and degassed for an hour. Subsequently, the obtained solution was cast on a glass plate, and the plate was immersed in deionized water. Thereafter, to extract the solvent from

the membrane pores, the fabricated membranes were soaked in water for 48 h.

Creighton method for synthesis and incorporation of AgNPs on SAN membrane

The Creighton method was modified by reduction of silver nitrate ($AgNO_3$, 100% purity), and used to synthesize the AgNPs. In this manner, Sodium borohydride (NaBH4, 99% purity) was applied, and the reaction was completed at 0 °C using an ice bath. Finally, the obtained colloid was refrigerated and samples were prepared for characterization using micro-Raman spectroscopy (Avantes, Netherlands) and UV–visible absorption spectrophotometry; herein, a 2150-UV spectrophotometer (UNICO, USA) was used.

To incorporate AgNPs into the SAN membrane, the reaction was completed at 0 °C in an ice bath, while the fabricated SAN membrane was covered with an NaBH4 solution [35, 36].

Figure 1 shows the purity of the Creighton colloid determined using micro-Raman spectroscopy. Only two characteristic Raman peaks can be observed during the bending and stretching of the H_2O vibrational modes. Therefore, we concluded that the AgNPs are free of organic contaminants. Figure 2 shows the UV–Visible absorption spectrum of the AgNPs. The entire fabrication process of the AgNP-incorporated SAN membrane is shown in Fig. 3. It illustrates that the synthesized AgNPs, using the Creighton method, are integrated onto the surface of the SAN membrane. This integration results in the accumulation of NPs on the membrane's surface, which enhances the membrane sites. In other words, the incorporation of AgNPs onto the SAN membrane leads to improve surface properties, which is beneficial for various applications. This technique has the potential to improve the performance of the SAN membrane and may be of interest to those working in the field of materials science.

Oil-in-water emulsion preparation

To prepare the dispersed oil phase for the oil-in-water (O/W) emulsion, oil and Tween 80 surfactant were mixed in distilled water at a mixing speed of 11,500 rpm for 30 min. The concentration of Tween 80 was 100 ppm. Particle size distribution (PSD) of the feed solutions was determined using the dynamic laser scattering (DLS) method (Nano ZS (red badge) ZEN3600, Malvern, UK). The PSD was measured twice; first during emulsion preparation and then after 4 h, which exceeded the required experimental time. It indicated a mean oil droplet diameter of approximately 0.15 µm with no significant variation during a certain period, showing stable emulsion during the experiments.

Antibacterial activity tests

Escherichia coli (gram-negative) and Staphylococcus aureus (gram-positive) were used as model bacteria to analyze membrane antibacterial activity. The membrane sheets were immersed in the cell suspension, which was

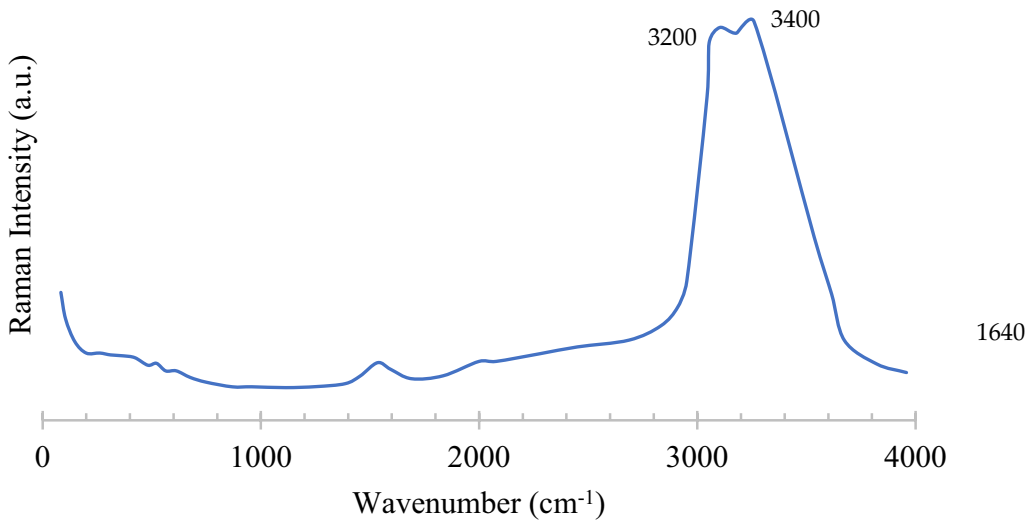

Fig. 1 Raman spectrum of AgNPs colloid

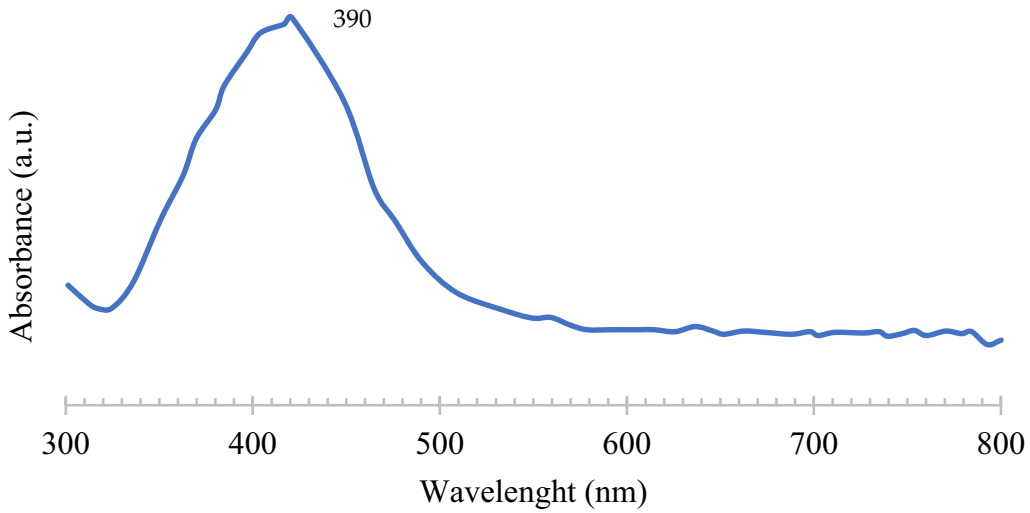

Fig. 2 UV–Visible absorption spectrum of the AgNPs

incubated on a shaker for 24 h at 35 °C. Finally, the colony-forming unit (CFU) procedure was used to quantify the viable cells in the solution. This measurement was performed thrice, and the average value was reported.

Membrane biofouling experiments

As the performance of SAN copolymer in membrane separation processes has not been yet investigated, the performance of the fabricated membranes can be investigated, according to the obtained characteristics, in the industrial oily wastewater treatment using the microfiltration process. Dynamic biofouling experiments were conducted in a cross-flow membrane module plant, and the feed containing Staphylococcus aureus or E. coli was reached at a pH of 7.4 and temperature of 25 °C. The oil concentration in all experiments is constant and is equal to 3000 mg/L. This oil concentration has a COD equivalent to 6350 ppm at pressure of 4 bar.

At the beginning of each test, the entire system was washed with ultrapure water, and the permeate flux was measured under the desired operating conditions. The feed was circulated in the system by the pump under operating conditions that were stabilized before each test; the process allows the retentate flow to return to the feed tank. The amount of permeate flux was measured by a digital scale and stored in the permeate tank. Before each test run, the membranes were placed in double-distilled water for at least 24 h, and the wet and swollen membranes were used in the performance test.

The module was washed using deionized water before the filtration process. Subsequently, the membrane was fixed using the module, process was run, and permeate flux was observed for 24 h. Finally, the membrane was carefully washed, and the process was repeated twice to measure the permeate flux after biofouling at pressure of 4 bar.

Membrane fouling is the reversible or irreversible accumulation of substances on the surface or inside membrane pores. If fouling is removed by backwashing, it is concluded that fouling is reversible; if chemical washing is needed to eliminate fouling, it is irreversible. As a result of fouling, the diameter of the membrane pores is reduced, which may lead to blockage. The accumulation of materials leads to the formation of layers on the surface of the membrane. These layers and materials that remain inside the membrane cause more resistance to the fluid flow.

Membrane fouling, which is a key obstacle in the widespread use of membrane processes, is caused by the accumulation of substances on the surface or in the membrane matrix, affecting membrane performance. This problem in the membrane separation process can be observed in four ways.

a) Standard blocking mechanism, including accumulation of particles on the inner surface of the membrane matrix pores. In this type of fouling, the pore radius is assumed to decrease with the accumulation of particles on the inner surface.
b) Cake filtration mechanism, wherein the particles accumulate on the membrane, causing pore fouling that is usually reversible and removable by washing.
c) Intermediate blocking mechanism, including the accumulation of particles in the membrane pores, in which the proportion of the membrane pores is inactive.

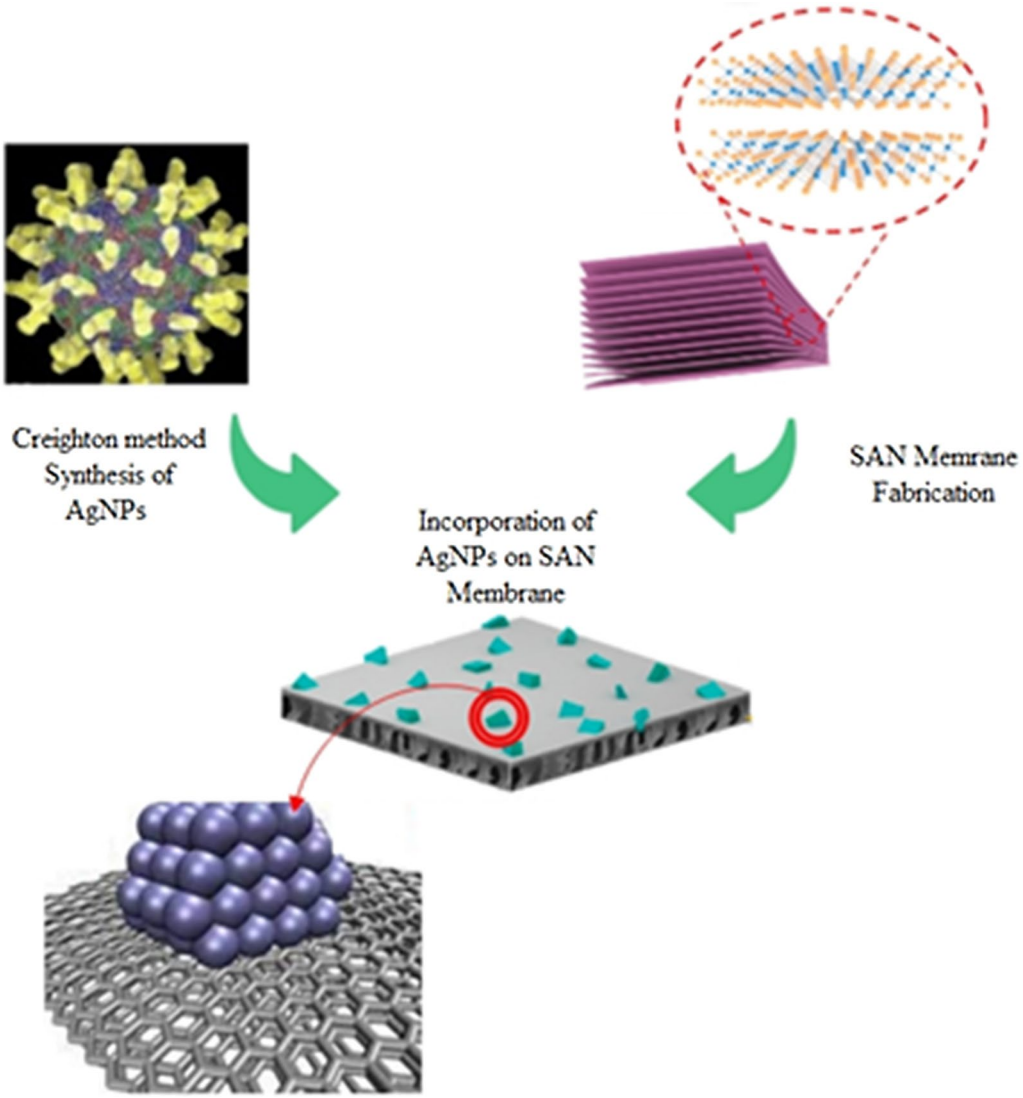

Fig. 3 Fabrication process of the AgNP-incorporated SAN membrane

d) Complete blocking mechanism, wherein the entrance of the pores is completely blocked by particles.

To check the flux reduction behavior of the fabricated membrane and antifouling properties, a filtration process at a constant pressure (1 bar) was used. First, the filtration process was performed with pure water for 60 min, and the permeate flux (J_0) was recorded. Subsequently, industrial wastewater was applied as the membrane feed, and the permeate flux (J_1) was recorded for 60 min. The fabricated membranes were then washed using distilled water for 30 min; thereafter, the membrane was removed from the module, and the membrane surface was washed gently. Finally, the amount of pure water permeated using the washed membrane was recorded over a period of 60 min (J_2), and the process was repeated in the subsequent cycles. At the beginning of each cycle, the feed solution was replaced with a new wastewater sample to maintain feed pollutant content. The permeability recovery of the membranes can be obtained using Eq. 1.

$$FRR\% = \frac{J_2}{J_0} \times 100 \tag{1}$$

To obtain the parameters of reversible membrane fouling (Rir), irreversible fouling (Rr), and total fouling (Rt), Eqs. 2, 3, and 4, respectively, were used.

$$Rir\% = \frac{(J_0 - J_2)}{J_0} \times 100 \tag{2}$$

$$Rr\% = \frac{(J_2 - J_1)}{J_0} \times 100 \tag{3}$$

$$Rt\% = \frac{J_0 - J_1}{J_0} \times 100 \tag{4}$$

To correctly predict the separation behavior in the membrane and subsequently design, simulate, and optimize the separation processes in membrane separation plants, the existence of a suitable thermodynamic model is necessary. The explanation and description of the behavior of the solutions by considering the physical and chemical differences of the components is possible only through thermodynamic solutions, and the development of suitable thermodynamic models that can correctly predict the behavior of wastewater treatment in membrane systems will be a turning point in understanding the behavior of such systems.

In this study, the interactions between the species in wastewater and fabricated membrane were correlated by applying the DLVO thermodynamic model. The interactions considered were electrostatic, van der Waals, and acid–base forces. The interaction energies between the species and membrane are presented in the DLVO model using the following equations:

$$\Delta G_{h_0}^{LW} = -2\left(\sqrt{\gamma_m^{LW}} - \sqrt{\gamma_w^{LW}}\right)\left(\sqrt{\gamma_s^{LW}} - \sqrt{\gamma_w^{LW}}\right) \tag{5}$$

$$\Delta G_{h_0}^{EL} = \frac{\varepsilon_r \varepsilon_0 \kappa}{2}\left(\zeta_s^2 + \zeta_m^2\right)\left(1 - \coth(\kappa h_0) + \frac{2\zeta_m \zeta_s}{\zeta_s^2 + \zeta_m^2}\operatorname{csch}(\kappa h_0)\right) \tag{6}$$

$$\Delta G_{h_0}^{AB} = 2\left[\begin{array}{l}\sqrt{\gamma_w^+}\left(\sqrt{\gamma_s^-} + \sqrt{\gamma_m^-} - \sqrt{\gamma_w^-}\right) + \\ \sqrt{\gamma_w^-}\left(\sqrt{\gamma_s^+} + \sqrt{\gamma_m^+} - \sqrt{\gamma_w^+}\right) - \sqrt{\gamma_s^-\gamma_m^+} - \sqrt{\gamma_s^+\gamma_m^-}\end{array}\right], \tag{7}$$

where the subscripts *m*, *w*, and *s* represent membrane, water, and wastewater species, respectively. The surface tensions of the electron donor, electron acceptor, and van der Waals forces are represented by γ+, γ-, and γ_{LW}, respectively.

Characterization of Membranes

Field Emission Scanning Electron Microscopes (FE-SEM, SU7000, Hitachi, Japan) were used to evaluate the morphology of the fabricated membranes. The membrane permeability recovery percentage can be attributed to the membrane surface roughness, such that the lower roughness of the membranes helps to improve the permeability recovery percentage. Atomic force microscopy (AFM) analysis was used to confirm this phenomenon. The membrane surface morphology was studied using the average roughness (SA) and difference between the lowest and highest peaks (Sz). To evaluate the arrangement of polymers in polymer solutions, determine the structure of polymer solutions, and check the order of polymer chains in the solution, the SAXS analysis is used. In this study, SAXS analysis was performed to investigate copolymer microphase separation in the system.

To measure the membrane porosity, membrane samples (80×150 mm) with known weights were first kept in water containing isopropanol for 52 h. Finally, their weights were measured again. The analysis was performed three times, and the membrane porosity was calculated using Eq. 8, where m_{dry} and m_{wet} are the weights of the dry and wet membranes, respectively. ρ, A, and L are the density of the pure liquid (kg · m $^{-3}$), area (m^2) of the sample, and sample thickness (m), respectively.

$$\varepsilon = \frac{m_{wet} - m_{dry}}{\rho A L} \tag{8}$$

In order to measure the pore size distribution of the fabricated membranes, Capillary Flow Porometry (CFP) method was used. In this method, a liquid is forced through a membrane under pressure, and the flow rate is measured. The Electronic Single-yarn Tensile Tester (at 20 °C, 0.450 m/min) was used to measure the tensile strength of the fabricated membranes.

To analyze the antibacterial activity of the membrane, Staphylococcus aureus and E. coli were applied as the model bacteria. The membrane sheets were immersed into the cell suspension with a concentration of 10^9 CFU/mL, and the CFU procedure was applied to quantify the viable cells in the obtained solution.

The CFU method is a widely used microbiological plating and counting method that estimates the number of viable microbial cells (bacteria, fungi, viruses, etc.) in a sample that are able to multiply via binary fission under controlled conditions. To measure the CFU, bacterial cultures are added to agar plates, often by serially diluting the original sample as it might be too concentrated to count. The number of visible colonies (CFU) present on an agar plate can be multiplied by the dilution factor to provide the CFU/ml value. The CFU method involves counting the number of visible colonies present on the plate to estimate the number of viable microbial cells

in the sample that are able to multiply via binary fission under controlled conditions. Bacterial colonies were counted after incubating the dishes at 25°C for 24 h. The test samples were spread-plated on LB medium with 1.5% agar in Petri dishes (two dishes per sample) and were serially diluted in sterile distilled water when necessary.

Finally, the CFU of control (%) is calculated (i.e. CFU (%) = Final count of the total number of cells in the sample after the process × 100 / Initial count of the total number of cells in the sample prior to the process).

To determine the amount of hydrophilicity and to check the changes in the surface energy of the fabricated membranes, a contact angle test of the water droplet was performed by placing 5 µL of deionized water on the surface of the fabricated membrane.

In this study, the pore size and pore distribution of the fabricated membranes, which determine both the degree of repulsion and permeability, were measured using the air bubble point (mostly in the micrometer range) and LLDP, and the results were verified using the SEM images. The SEM image can be analyzed to measure the pore size of the fabricated membranes using digitizer software.

Results and discussion

Membrane attributes

Figure 4 shows the SEM images of the neat and AgNP-incorporated SAN membranes. The AgNPs are seen on the membrane surface and in the membrane pores.

The membrane pore sizes and fabricated membrane porosities are listed in Table 1. It is seen that as the pore size of the membrane increased, the porosity also increased. It has also been reported that increasing the concentration of AgNPs initially reduces the porosity and permeability. Nevertheless, increasing the number of nanoparticles to more than the optimal amount decreases the porosity and permeability. Furthermore, it was found that an increase in AgNPs initially enhanced the mechanical strength and bulk density of the neat membrane. The thicknesses of the fabricated membranes were also measured and are listed in Table 1. The thickness of the obtained membranes followed the same behavior as the membrane pore size and porosity. This phenomenon could be due to the formation of nanoparticle clusters that impede the flow of water through the membrane. Additionally, increasing the number of nanoparticles beyond the optimal amount could lead to agglomeration or aggregation, which can reduce the overall effectiveness of the membrane. Therefore, it is important to carefully control the concentration of AgNPs to ensure optimal membrane performance.

Table 1 Thickness, porosity, and pore size of the fabricated membranes

	AgNPs amount (g)	Porosity	Pore Size (µm)	Thickness (µm)
M1	0	0.85 ± 0.01	3.5 ± 0.2 µm	185 ± 2 µm
M2	1	0.79 ± 0.03	2.9 ± 0.1 µm	173 ± 1 µm
M3	1.5	0.71 ± 0.02	2.4 ± 0.1 µm	162 ± 2 µm
M4	2	0.64 ± 0.02	2.1 ± 0.3 µm	133 ± 2 µm
M5	2.5	0.69 ± 0.03	2.6 ± 0.2 µm	143 ± 2 µm
M6	3	0.75 ± 0.01	2.8 ± 0.2 µm	162 ± 3 µm
M7	4	0.81 ± 0.02	3.2 ± 0.1 µm	188 ± 1 µm
M8	10	0.84 ± 0.02	3.6 ± 0.1 µm	201 ± 1 µm

The tensile strengths of the membranes with different amounts of $AgNO_3$ are shown in Fig. 5. Increasing the amount of AgNPs initially enhances the mechanical strength; however, increasing the amount of nanoparticles beyond the optimal value can decrease the mechanical strength.

The tensile strength increased from 124 to 341 kPa when the amount of AgNPs was increased from 1 to

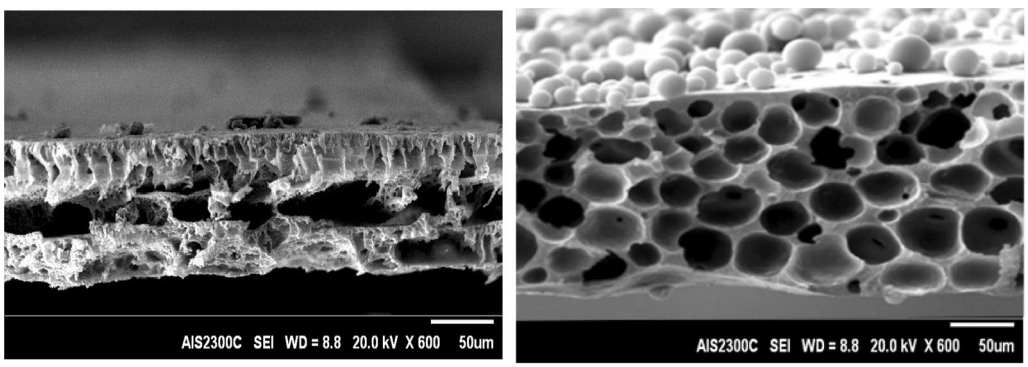

Fig. 4 SEM images of the **a** neat SAN membrane and **b** AgNP-incorporated SAN membrane

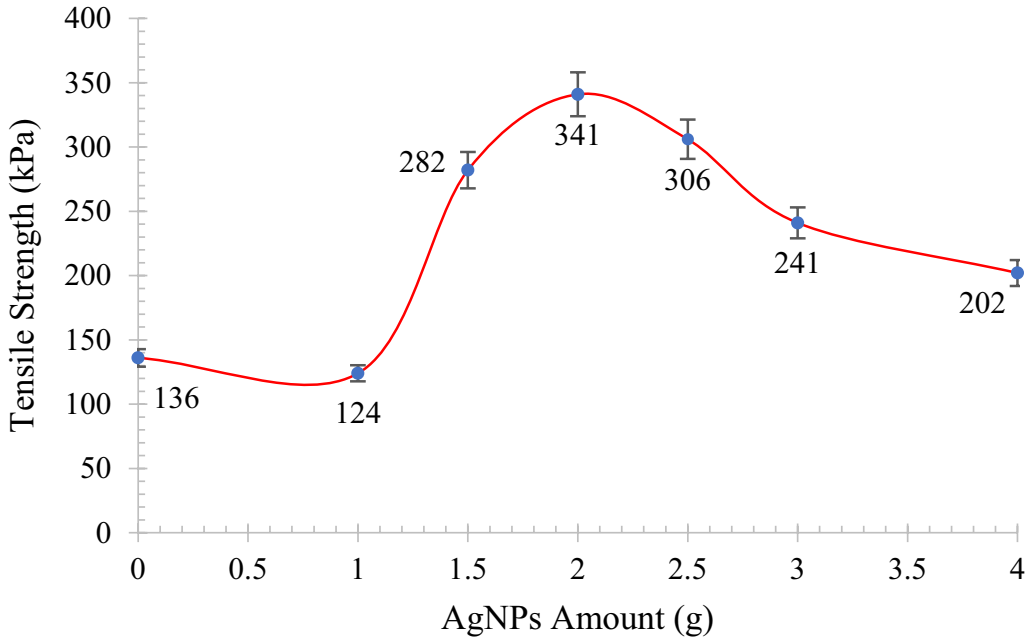

Fig. 5 Tensile strength of SAN copolymer membranes using different $AgNO_3$ amount

2 g (Fig. 5). Moreover, the membrane tensile strength decreased to 202 kPa when the AgNPs were increased to 4 g in the fabricated membrane matrix. The increase in the tensile strength of the membrane can be attributed to the complex structure of the fabricated membranes, which increasingly interacts with the AgNPs. This complex structure increases the tensile strength when AgNPs up to 2 g were added; thereafter, the tensile strength decreases with the addition of more AgNPs to the membrane matrix.

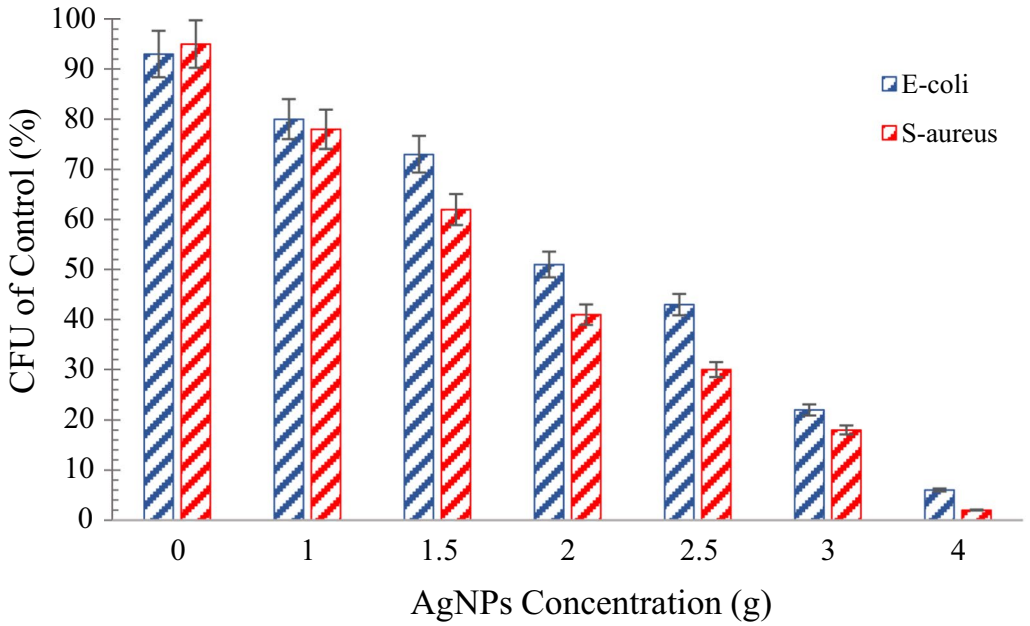

Fig. 6 Antimicrobial properties in terms of CFU of the fabricated membranes using different amount of AgNPs, after exposure to the Staphylococcus aureus and the E. coli cells for 12 h at 35 °C

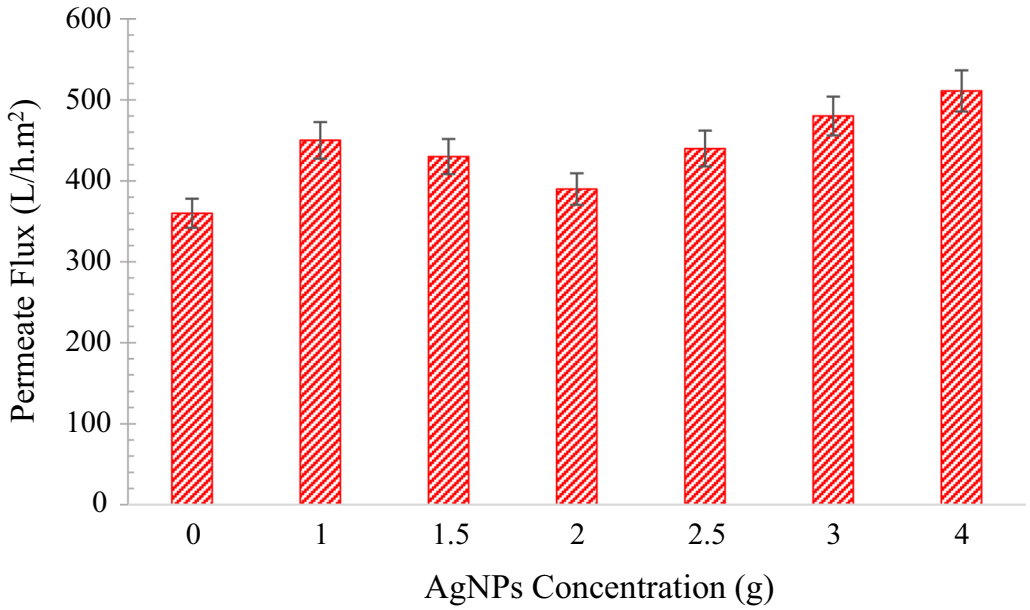

Fig. 7 Permeate flux (L/m^2.h) of the obtained membranes using different concentration of AgNPs at pressure of 2 bar and duration of 60 min

Antibacterial activity tests

Figure 6 shows the antimicrobial properties in terms of CFU of the fabricated membranes using different amounts of AgNPs after exposure to Staphylococcus aureus and E. coli cells for 12 h at 35 °C.

The results show that with an increase in the amount of AgNPs in the membrane matrix, the percentage of CFU decreases; the CFU% for the Staphylococcus aureus and the E.coli reached 2% and 6%, respectively. The membranes with higher porosity resulted in a higher removal of bacteria than the membranes with lower porosity.

Membrane micro-filtration pilot test

The permeabilities of the membranes obtained using different concentrations of AgNPs are shown in Fig. 7. Increasing the AgNP concentration initially decreased

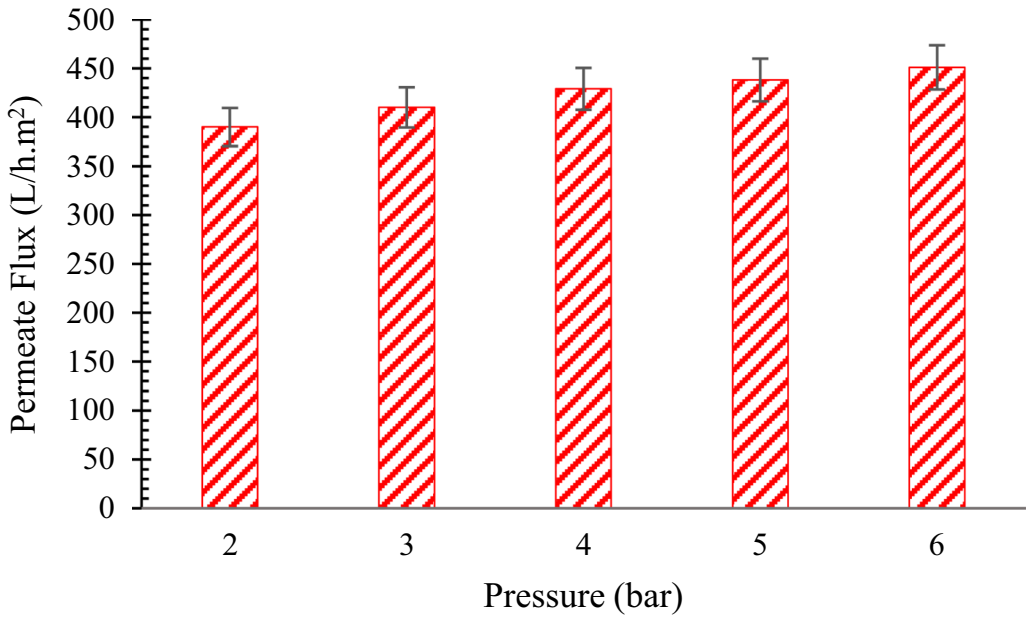

Fig. 8 Obtained permeate flux of the fabricated M4 membrane (L/m^2.h) at different pressures of the feed flow

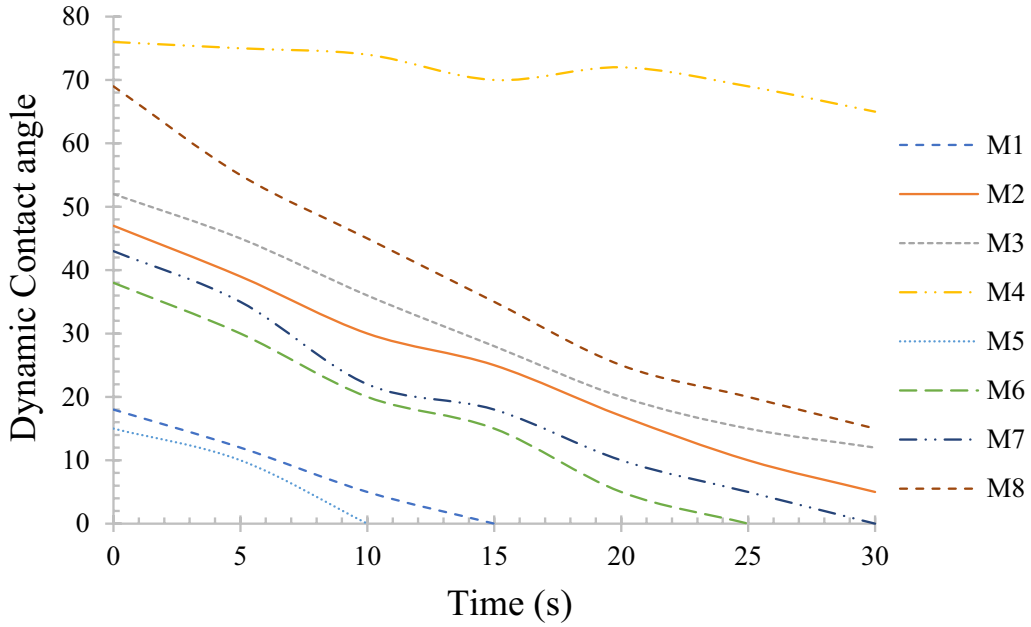

Fig. 9 Dynamic analysis of the contact angle of water with the membrane surface. Note that the unit of dynamic contact angle is degree

the permeate flux of the membrane to 390 L/m^2.h; however, the permeate flux could be increased by further increasing the amount of AgNPs. The results show that the permeate flux can be obtained as 450 L/m^2.h using 1 g of AgNPs, and the maximum flux can be obtained as 511 L/m^2.h using 4 g of AgNPs.

The effects of feed pressure and feed rate on permeate flow were also investigated, and the results are shown in Fig. 8. The permeate flux can be increased from 390 to 451 L/m^2.h by increasing the pressure from 2 to 6 bar. It is evident that the permeate flux can also be increased by increasing the feed flow rate. The chemical oxygen demand (COD) of the resulting permeate fluxes in all the experiments was greater than 99.5%.

The antibiofouling behavior of the fabricated membrane was investigated in a cross-flow filtration pilot plant using a feed solution containing E. coli and Staphylococcus aureus suspensions.

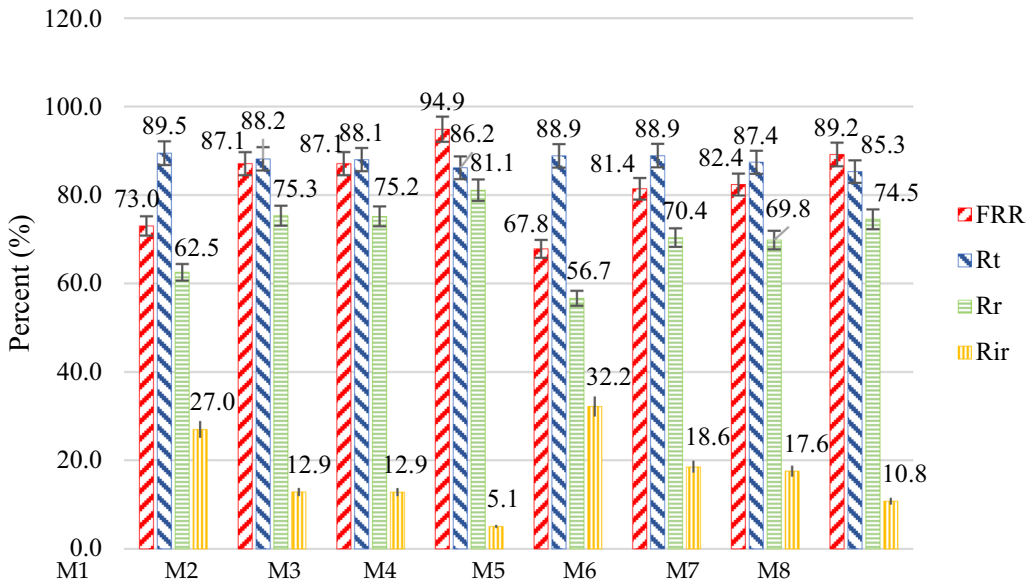

Fig. 10 Fouling rate and permeability recovery percentage of different fabricated membranes

To check the flux reduction behavior and antifouling properties of the fabricated membranes, a filtration process at constant pressure was applied. In this method, the filtration process test was performed with pure water for 60 min, and the permeate flux was measured. Industrial wastewater was used as the feed, and the permeate flux was also investigated in 60 min. The fabricated membranes were then washed using distilled water for 30 min; thereafter, the membrane was removed from the module, and the membrane surface was washed gently. Finally, the amount of permeate flux, using wastewater as the feed, was recorded using the washed membrane over a period of 60 min, and the above-mentioned process was repeated in the subsequent cycles. At the beginning of each cycle, the feed solution was replaced by fresh wastewater.

The permeate flux with AgNP amount of 2 g was considered as an example during the filtration process in each cycle. After each cycle, the amount of purified water flux decreased to a very small amount. This phenomenon can be related to internal membrane pore fouling. Therefore, biofouling of the membrane surface or membrane matrix pores can decrease the permeate flux, which is irreversible fouling.

Contact angle of water drop

A dynamic analysis of the water contact angle with the surface of the fabricated membranes over time is presented in Fig. 9. The water contact angle of M4 is observed to be more constant during time compared to the other membranes, and it has a significant difference with them. This observation can be attributed to the fact that the M4 membrane has the best performance, in which 2 g AgNPs was applied. Nevertheless, there is no significancy between other membranes using different amounts of silver nanoparticles. The constant water contact angle of M4 membrane suggests that it is more effective in repelling water over time compared to the other membranes. This observation is significant as it provides insight into the effectiveness of the different membranes in purifying water.

This observation suggests that the amount of nanoparticles used in the fabrication of the membranes may not be the only factor affecting their performance. Therefore, further studies are needed to identify other factors that may contribute to the effectiveness of the membranes in purifying water.

Pore size and pore distribution

The size of the droplets in the industrial wastewater used as feed was checked using the DLS analysis in the

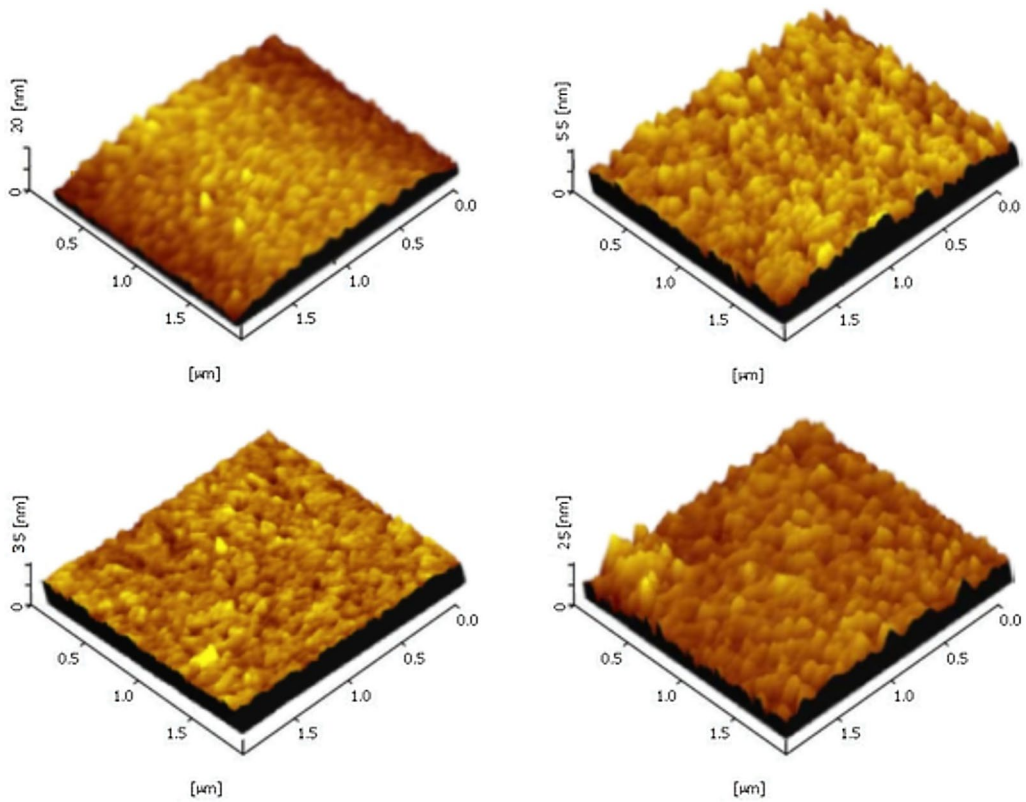

Fig. 11 AFM analysis and average surface roughness of the fabricated membranes

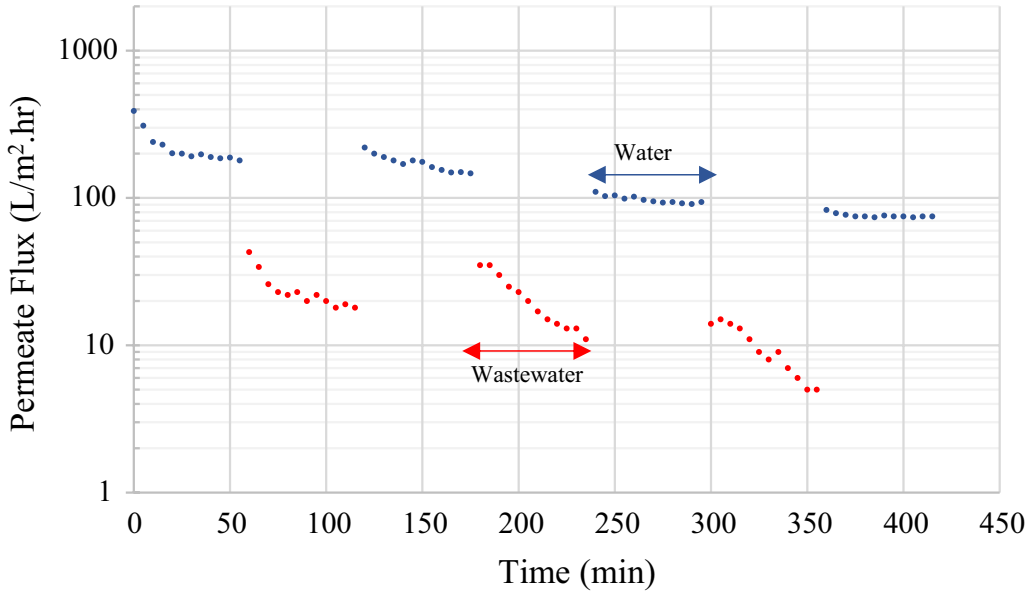

Fig. 12 Water permeate flux of the fabricated M4 membrane during the filtration process in three cycles at pressure of 2 bar

range of 0–10 µm, and the results showed that approximately 90% of the droplets had a size in the range of 390–450 nm, and the remaining 10% were the range of 270–290 nm.

Membrane fouling analysis

The results presented in Fig. 10 show that the fouling amount and recovery percentage of the permeability of the fabricated membranes are affected by the hydrophilicity of the membrane. As the hydrophilicity of the membrane decreases, the fouling is reduced, and vice versa. This finding is consistent with previous research on membrane fouling, which has identified various factors affecting fouling, including the type of fouling, and membrane surface chemistry. This is due to the fact that the hydrophilic membranes have a higher affinity for water, which reduces the interaction between the membrane and foulants, leading to less deposition of foulants on the membrane surface and/or pores. In contrast, hydrophobic membranes repel water, which increases the interaction between the membrane and foulants, leading to more deposition of foulants on the membrane surface and/or pores. The intermolecular interactions between the foulant and the membrane surface are also affected by the hydrophilicity of the membrane. As the hydrophilicity of the membrane decreases, the surface becomes more hydrophobic, which increases the interaction between the membrane and foulants, leading to more deposition of foulants on the membrane surface and/or pores. Therefore, reducing the hydrophilicity of the membrane can increase the fouling of the membrane, while increasing the hydrophilicity can reduce the membrane fouling. A recent study explored the relative impact of charge and hydrophilicity on the anti-fouling properties of polyester membranes and found that charge impacts the anti-fouling potential more significantly than hydrophilicity. Understanding the interplay between charge and hydrophilicity can help guide the synthesis of more effective anti-fouling membranes.

Table 2 Surface tension parameters of DLVO thermodynamic model

	γ^+	γ^-	γ^{LW}
M1	0.22	8.66	43.28
M2	0.21	12.8	44.8
M3	0.32	13.2	42.93
M4	0.29	24.32	41.39
M5	0.26	3.29	43.48
M6	0.24	11.1	47.66
M7	0.23	12.28	45.4

Figure 11 shows the AFM analysis results and average surface roughness of the fabricated membranes. These results were also confirmed by comparing the size of the contact angle; the results showed that the contact angle and fouling decreased with an increase in the membrane roughness.

Figure 12 shows the permeate water flux of the fabricated M4 membrane during the filtration process at pressure of 2 bar for each cycle. After each cycle, the purified water flux decreased to a very small amount. This can be attributed to internal membrane pore fouling. Owing to

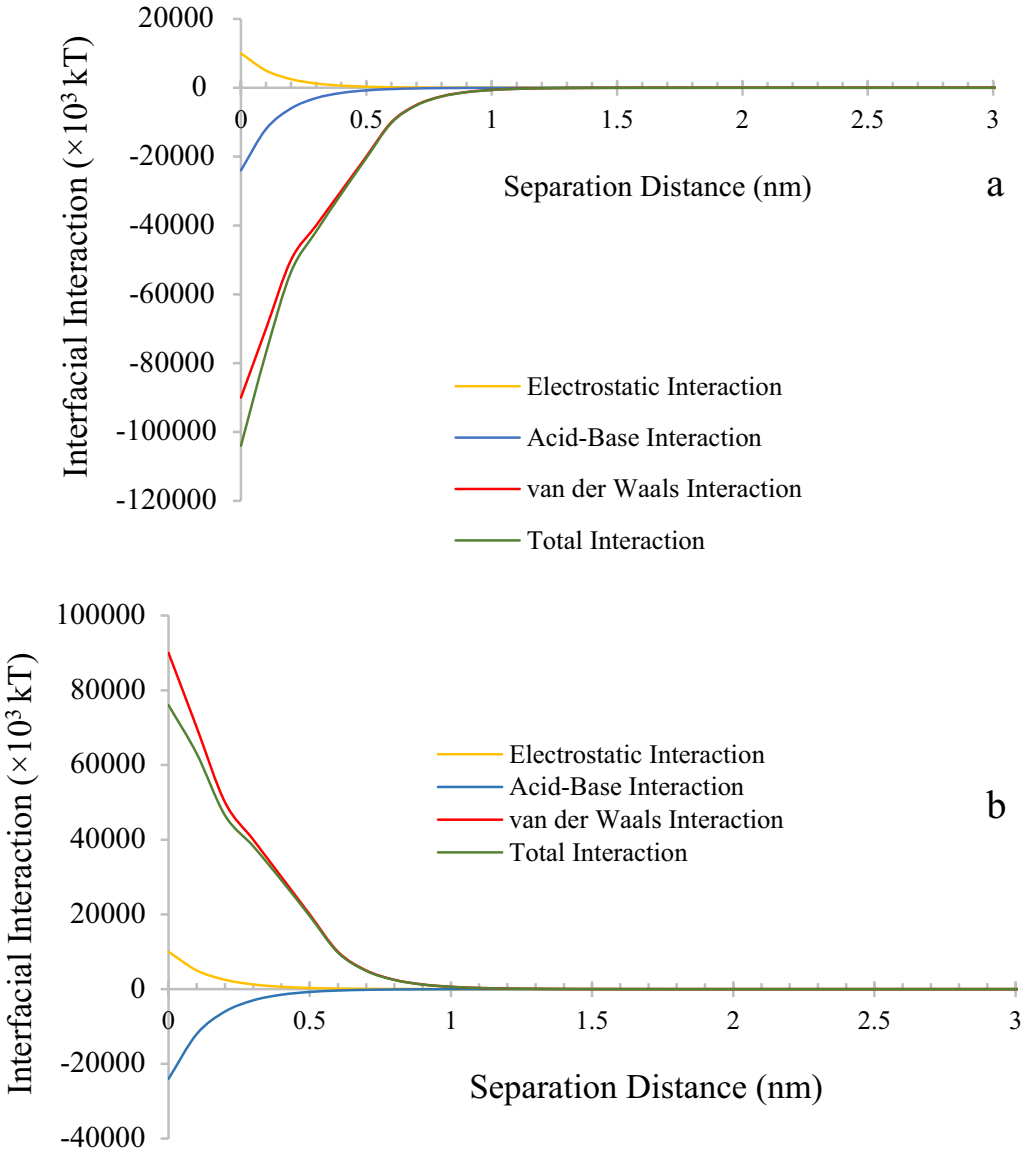

Fig. 13 Interaction energy between the fabricated membranes and E.coli; **a** M1 membrane and **b** M4 membrane

the high amount of pollutants in the feed, the adhesion and expansion of the droplets in the inner pores of the membrane cause narrowing of the flow channels; in some cases, it blocks the membrane pores and causes complete fouling. Therefore, the flux decrease can be related to irreversible fouling caused by the strong binding of the droplets to the surface of the membrane or inside the pores.

Antifouling mechanism

The surface tension parameters of the DLVO thermodynamic model are presented in Table 2. As shown in Table 2, M4 has more negative charge and thus the highest amount of hydrophobicity; whereas, M5 shows the lowest amount of negative charge and thus the highest amount of hydrophilic property. The obtained results are in full agreement with the data presented in Fig. 10, indicating that the FRR increases as the negative charge of the membrane increases.

Figure 13 shows the interaction energy between the fabricated membranes and E. coli. In Fig. 13a, the interaction energy between M1 membrane (with no silver nanoparticles in the membrane matrix) and E. coli shows a negative value, indicating that the interaction between SAN and E. coli is thermodynamically attractive. Therefore, it can be concluded that in M1 membrane, E. coli can adhere to the membrane to form a fouling layer, blocking the pores and leading to membrane biofouling.

In contrast, it can be seen in Fig. 13b that the total energy between the pollutant species and M4 membrane is positive, which indicates that the adhesion of E.coli particles on the membrane surface of M4 membrane is thermodynamically unfavorable. Thus, M4 membrane has antifouling properties, as indicated by the highest FRR. Therefore, the use of AgNPs can improve the antifouling properties of the membrane. Applying a small amount of AgNPs reduced the amount of membrane fouling to a great extent; however, the use of AgNPs has an optimal limit, and if used in excess, it will reduce the antifouling property of the membrane.

Conclusions

In this study, a new low-cost microfiltration membrane was prepared by incorporating AgNPs on a poly (acrylonitrile-styrene) membrane, where the AgNPs were synthesized using the Creighton method. The obtained copolymer membranes were studied, characterized, and investigated by SEM, infrared vibrational spectroscopy, and ultraviolet–visible spectroscopy. The effects of the amount of AgNPs on the morphology, pore size, porosity, mechanical strength, and permeability were studied. Increasing the amount of AgNPs initially enhanced the mechanical strength and selectivity of the neat membrane; however, it also decreased its permeability and porosity. Nevertheless, increasing the amount of nanoparticles beyond the optimal amount caused a decrease in the mechanical strength and increased the porosity and permeability. To check the flux reduction behavior of the fabricated membrane and antifouling properties, a filtration process at constant pressure was applied. The hydrophilicity of the membrane decreased, fouling decreased, and vice versa. Moreover, the permeate flux during the filtration process was studied in three cycles, and the amount of purified water flux decreased after each cycle to a very small amount, which can be related to membrane internal fouling. Owing to the high amount of pollutants in wastewater, the oil droplets in the membrane pores caused complete pore blocking. Therefore, the decrease in permeate flux can be attributed to irreversible fouling caused by the strong binding of droplets to the surface of the membrane or inside the membrane pores. The lower roughness of the membranes improves the permeability recovery percentage because the membrane permeability recovery percentage can be attributed to the membrane surface roughness. The results showed that increasing the membrane roughness can decrease the contact angle and membrane fouling. Furthermore, to determine the amount of hydrophilicity and check the changes in the surface energy of the fabricated membranes, a water droplet contact angle analysis was performed. The results showed that poly(acrylonitrile-styrene) copolymer membranes containing AgNPs have promising wastewater treatment applications.

Acknowledgements
This work was supported by the King Khalid University, Abha, Saudi Arabia. The authors extend their appreciation to the Deanship of Scientific Research at King Khalid University for funding this work through Large Groups Project under grant number R.G.P. 2/57/44.

Author contributions
Conceptualization, methodology, software: All authors; investigation and visualization: AEJ, AA, DS; data curation; AEJ, DS, MM; validation: NA-A, SSS; AA, AS; writing—original draft preparation; All authors; Writing—review & editing, AA, MAU, MS, AS, NA-A. All authors have read and agreed to the published version of the manuscript.

Funding
Open access funding was provided by Lulea University of Technology.

Availability of data and materials
Not applicable.

Declarations

Ethics approval and consent to participate
Not applicable.

Consent for publication
Not applicable.

Competing interests
The authors declare no conflict of interest.

Author details
[1]Department of Chemical Engineering, College of Engineering, King Khalid University, Abha 61421, Saudi Arabia. [2]Department of Civil and Environmental Engineering, Islamic University of Technology (IUT), Gazipur, Bangladesh. [3]Department of Civil and Construction Engineering, Swinburne University of Technology, Melbourne, Australia. [4]Department of Civil Engineering, College of Engineering, University of Diyala, Diyala Governorate, Iraq. [5]Research Institute of Sciences and Engineering, University of Sharjah, Sharjah, United Arab Emirates. [6]Department of Civil & Environmental Engineering, University of Sharjah, Sharjah, United Arab Emirates. [7]Department of Chemistry, Faculty of Science, S.P. College Sirohi City, Sirohi, Rajasthan 307001, India. [8]Azogues Campus Nursing Career, Health and Behavior Research Group (HBR), Psychometry and Ethology Laboratory, Catholic University of Cuenca, Cuenca, Ecuador. [9]Epidemiology and Biostatistics Research Group, CES University, Medellin, Colombia. [10]Educational Statistics Research Group (GIEE), National University of Education, Loja, Ecuador. [11]Department of Civil Engineering, College of Engineering, Jouf University, Sakaka 42421, Saudi Arabia. [12]Department of Computer Science, Al-Turath University College, Al Mansour, Baghdad, Iraq. [13]Department of Civil Engineering, College of Engineering, Qassim University, Buraidah 51452, Saudi Arabia. [14]Civil, Environmental and Natural Resources Engineering, Lulea University of Technology, 971 87 Lulea, Sweden.

Received: 11 March 2023 Accepted: 11 July 2023
Published online: 13 August 2023

References

1. Quang DV, Sarawade PB, Jeon SJ, Kim SH, Kim J-K, Chai YG, Kim HT (2013) Effective water disinfection using silver nanoparticle containing silica beads. Appl Surf Sci 266:280–287
2. Ferreira AM, Roque ÉB, da Fonseca FV, Borges CP (2015) High flux microfiltration membranes with silver nanoparticles for water disinfection. Desalination Water Treat 56:3590–3598
3. Shi X, Tal G, Hankins NP, Gitis V (2014) Fouling and cleaning of ultrafiltration membranes: a review. J Water Process Eng 1:121–138
4. Hamta A, Mohammadi A, Dehghani MR, Feyzi F (2018) Liquid-liquid equilibrium and thermodynamic modeling of aqueous two-phase system containing polypropylene glycol and NaClO 4 at T=(288.15 and 298.15) K. J Solution Chem 47:1–25

5. Zeman L, Tkacik G (1988) Thermodynamic analysis of a membrane-forming system water/N-methyl-2-pyrrolidone/polyethersulfone. J Memb Sci 36:119–140
6. Rashid KT, Rahman SBA (2006) Enhancement the flux of PVDF-CO-HFP hollow fiber membranes for direct contact membrane distillation applications. 2006.
7. Shahmirzadi MAA, Kargari A (2018) Nanocomposite membranes. In: emerging technologies for sustainable desalination handbook; Elsevier, pp 285–330.
8. Hamta A, Ashtiani FZ, Karimi M, Sadeghi Y, MoayedFard S, Ghorabi S (2021) Copolymer membrane fabrication for highly efficient oil-in-water emulsion separation. Chem Eng Technol 44:1321–1326
9. Zhang L, Graham N, Li G, Yu W (2022) Divergent accumulation of membrane biofouling by slight elevation of nitrogen and phosphorus in drinking water treatment: performances and mechanisms. Water Res 222:118898
10. Abushaban A, Salinas-Rodriguez SG, Philibert M, le Bouille L, Necibi MC, Chehbouni A (2022) Biofouling potential indicators to assess pretreatment and mitigate biofouling in SWRO membranes: a short review. Desalination 527:115543
11. Pasternak G, de Rosset A, Tyszkiewicz N, Widera B, Greenman J, Ieropoulos I (2022) Prevention and removal of membrane and separator biofouling in bioelectrochemical systems-a comprehensive review. IScience 25:104510
12. Hamta A, Ashtiani FZ, Karimi M, Moayedfard S (2022) Asymmetric block copolymer membrane fabrication mechanism through self-assembly and non-solvent induced phase separation (SNIPS) process. Sci Rep 12:1–10
13. Prince JA, Bhuvana S, Anbharasi V, Ayyanar N, Boodhoo KVK, Singh G (2014) Self-cleaning metal organic framework (mof) based ultra filtration membranes-a solution to bio-fouling in membrane separation processes. Sci Rep 4:1–9
14. Hamta A, Dehghani MR, Gholami M (2017) Novel experimental data on aqueous two-phase system containing PEG–6000 and Na2CO3 at T=(293.15, 303.15 and 313.15) K. J Mol Liq 241:144–149
15. Hamta A, Zokaee Ashtiani F, Karimi M, Safikhani A (2020) Manipulating of polyacrylonitrile membrane porosity via SiO2 and TiO2 nanoparticles: thermodynamic and experimental point of view. Polym Adv Technol. https://doi.org/10.1002/pat.5138
16. Kalhapure RS, Sonawane SJ, Sikwal DR, Jadhav M, Rambharose S, Mocktar C, Govender T (2015) Solid lipid nanoparticles of clotrimazole silver complex: an efficient nano antibacterial against *Staphylococcus aureus* and MRSA. Colloids Surf B Biointerfaces 136:651–658
17. Krishnaraj C, Ramachandran R, Mohan K, Kalaichelvan PT (2012) Optimization for rapid synthesis of silver nanoparticles and its effect on phytopathogenic fungi. Spectrochim Acta A Mol Biomol Spectrosc 93:95–99
18. Borrego B, Lorenzo G, Mota-Morales JD, Almanza-Reyes H, Mateos F, López-Gil E, de la Losa N, Burmistrov VA, Pestryakov AN, Brun A (2016) Potential application of silver nanoparticles to control the infectivity of rift valley fever virus in vitro and in vivo. Nanomedicine 12:1185–1192
19. Ren D, Smith JA (2013) Retention and transport of silver nanoparticles in a ceramic porous medium used for point-of-use water treatment. Environ Sci Technol 47:3825–3832
20. Danilczuk M, Lund A, Sadlo J, Yamada H, Michalik J (2006) Conduction electron spin resonance of small silver particles. Spectrochim Acta A Mol Biomol Spectrosc 63:189–191
21. Sondi I, Salopek-Sondi B (2004) Silver nanoparticles as antimicrobial agent: a case study on *E. Coli* as a model for gram-negative bacteria. J Colloid Interface Sci 275:177–182
22. Zamel D, Khan AU (2021) Bacterial immobilization on cellulose acetate based nanofibers for methylene blue removal from wastewater: mini-review. Inorg Chem Commun 131:108766
23. Behboudi A, Jafarzadeh Y, Yegani R (2018) Enhancement of antifouling and antibacterial properties of PVC hollow fiber ultrafiltration membranes using pristine and modified silver nanoparticles. J Environ Chem Eng 6:1764–1773
24. Linhares AMF, Grando RL, Borges CP, da Fonseca FV (2018) Technological prospection on membranes containing silver nanoparticles for water disinfection. Recent Pat Nanotechnol 12:3–12
25. Islam MS, Naz AN, Alam MN, Das AK, Yeum JH (2020) Electrospun poly (Vinyl Alcohol)/silver nanoparticle/carbon nanotube multi-composite nanofiber mat: fabrication, characterization and evaluation of thermal, mechanical and antibacterial properties. Colloid Interface Sci Commun 35:100247
26. Kim J, Yun E-T, Tijing L, Shon HK, Hong S (2022) Mitigation of fouling and wetting in membrane distillation by electrical repulsion using a multi-layered single-wall carbon nanotube/polyvinylidene fluoride membrane. J Memb Sci 653:120519
27. Al-Gharabli S, El-Rub ZA, Hamad EM, Kujawski W, Flanc Z, Pianka K, Jankowski W, Kujawa J (2022) Toward anti-fouling properties and enhanced performance in separation process-carbon nanotubes-PVDF hybrids. Appl Surf Sci 602:154341
28. Nath A, Shah A, Singh LR, Mahato M (2021) Waste plastic-derived NiO-MWCNT composite as visible light photocatalyst for degradation of methylene blue dye. Nanotechnol Environ Eng 6:1–14
29. Werner JG, Lee H, Wiesner U, Weitz DA (2021) Ordered mesoporous microcapsules from double emulsion confined block copolymer self-assembly. ACS Nano 15:3490–3499
30. Afshina S, Poureshgha Y, Rashtbaria Y, Fazlzadehb M, Aslc FB, Hamzezadeha A, Pormazard SM (2021) Eco-friendly cost-effective approach for synthesis of ZnO nanoparticles and loaded on worn tire powdered activated carbon as a novel adsorbent to remove organic dyes from aqueous solutions: equilibrium, kinetic, regeneration and thermodynamic study. Desalination Water Treat 227:391–403
31. Yu L, Han M, He F (2017) A review of treating oily wastewater. Arab J Chem 10:S1913–S1922
32. Adetunji AI, Olaniran AO (2021) Treatment of industrial oily wastewater by advanced technologies: a review. Appl Water Sci 11(6):98
33. Roy S, Bhalani DV, Jewrajka SK (2020) Surface segregation of segmented amphiphilic copolymer of poly (dimethylsiloxane) and poly (ethylene glycol) on poly (vinylidene fluoride) blend membrane for oil-water emulsion separation. Sep Purif Technol 232:115940
34. Wang N, Wang T, Hu Y (2017) Tailoring membrane surface properties and ultrafiltration performances via the self-assembly of polyethylene glycol-block-polysulfone-block-polyethylene glycol block copolymer upon thermal and solvent annealing. ACS Appl Mater Interfaces 9:31018–31030
35. Heydari M, Gharagozlou M, Ghahari M (2021) Synthesis and application of nanocomposite containing metal-organic framework and magnetic nanoparticles in silica matrix for decolorization of methylene blue. J Color Sci Technol 15:103–115
36. Hołda AK, Vankelecom IFJ (2015) Understanding and guiding the phase inversion process for synthesis of solvent resistant nanofiltration membranes. J Appl Polym Sci. https://doi.org/10.1002/app.42130

Publisher's Note